*Geological Magazine*

**www.cambridge.org/geo**

# Detrital Sr–Nd isotopes, sediment provenances and depositional processes in the Laxmi Basin of the Arabian Sea during the last 800 ka

Boo-Keun Khim[1], Keiji Horikawa[2], Yoshihiro Asahara[3], Ji-Eun Kim[1] and Minoru Ikehara[4]

[1]Department of Oceanography, Pusan National University, Busan 46241, Korea, [2]Graduate School of Science and Engineering for Research, University of Toyama, Toyama 930-8555, Japan, [3]Department of Earth and Environmental Sciences, Nagoya University, Nagoya 464-8601, Japan and [4]Center for Advanced Marine Core Research, Kochi University, Nankoku 783-8502, Japan

**Original Article**

**Cite this article:** Khim B-K, Horikawa K, Asahara Y, Kim J-E, and Ikehara Minoru (2020) Detrital Sr–Nd isotopes, sediment provenances and depositional processes in the Laxmi Basin of the Arabian Sea during the last 800 ka. *Geological Magazine* **157**: 895–907. https://doi.org/10.1017/S0016756818000596

Received: 30 January 2018
Revised: 8 July 2018
Accepted: 11 July 2018
First published online: 23 November 2018

**Keywords:**
sediment provenance; Sr–Nd isotope; Indus Fan; Pleistocene; IODP

**Author for correspondence:** Boo-Keun Khim, Email: bkkhim@pusan.ac.kr

**Abstract**

$^{87}Sr/^{86}Sr$ ratios and εNd values of detrital particles at International Ocean Discovery Program (IODP) Site U1456 in the Laxmi Basin of the Arabian Sea were measured to trace changes in sediment provenance over glacial–interglacial cycles. Based on the correlation of planktonic foraminiferal (*Globigerinoides ruber*) $\delta^{18}O$ fluctuations with the LR04 stack of benthic foraminifera $\delta^{18}O$ values, combined with shipboard biostratigraphic and palaeomagnetic data, the studied interval spans ~1.2 Ma. Over the past 800 ka, $^{87}Sr/^{86}Sr$ values ranged from 0.711 to 0.726 while εNd values ranged between −12.5 and −7.3 in the detrital particles. By comparing $^{87}Sr/^{86}Sr$ ratios and εNd values of the possible sources of river sediments with our data, we found that sediments in the Laxmi Basin were influenced to various degrees by proportions of at least three sediment sources (i.e. Tapi River, Narmada River and Indus River). The Indus River might be a more important contributor to glacial sediments. Although $^{87}Sr/^{86}Sr$ ratios and εNd values varied quasi-cyclically, this pattern did not correspond precisely to the glacial–interglacial cycles. In particular, low-magnetic-susceptibility (low-MS) intervals coinciding with pelagic carbonates were characterized by low $^{87}Sr/^{86}Sr$ ratios and high εNd values, whereas high-MS intervals matching turbidite deposits showed high $^{87}Sr/^{86}Sr$ ratios and low εNd values. Thus, this study reveals that differences in the depositional processes between glacial and interglacial periods, governed by changes in sea level and monsoon activity, are an important factor in deciding $^{87}Sr/^{86}Sr$ ratios and εNd values of the detrital fraction in the Indus Fan of the Arabian Sea.

## 1. Introduction

The Arabian Sea is dominated by a monsoon climate characterized by seasonal reversal of winds and precipitations, which results in large seasonal oceanographic changes in seawater properties and sediment distribution (Nair *et al.* 1989). In general, the Arabian Sea is strongly influenced by the SW monsoon (June–September), and moderately influenced by the NE monsoon (December–February) and the associated reversal of the surface currents (Mooley & Parthasarathy, 1984). The SW monsoon accounts for the majority of the rainfall (>3000 mm) in India (the Karakoram and the Himalayas), whereas the NE monsoon is less important in terms of precipitation, although Karim & Veizer (2002) reported that a high proportion of the Indus discharge waters must have originated from the Mediterranean on the basis of isotope mass balance. During the SW monsoon, the prevailing southwesterly winds also induce the strong longshore current. But the longshore sediment transport seems limited within the inner continental shelf at the present time (Shanas & Kumar, 2014), although longshore transport may have played a more effective role in delivering sediments to the deep sea during the glacial periods when the sea level was low. The deep sea sediments in the Arabian Sea are known to be transported from several sources. The most important sediment fractions to these sources are fluvial detritus from the Indian continent and Somalia, aeolian particles from Arabia, and submarine weathering products of the Carlsberg Ridge (Milliman *et al.* 1984; Shankar *et al.* 1987; Sirocko & Sarnthein, 1989; Alagarsamy & Zhang, 2005; Chandramohan & Balchand, 2007).

The contribution of terrigenous particles to the Arabian Sea is largely controlled by monsoon activity and its effects on precipitation and riverine discharge (Haake *et al.* 1993). Analogously to the situation in the Bay of Bengal, several rivers draining peninsular India discharge their freshwater into the Arabian Sea: the Indus, Narmada and Tapti Rivers, as well as small rivers from the Western Ghats (Fig. 1). The Indus River may be the oldest continuously active river in the Himalayan region. It has been flowing from its origin in the Indus Suture Zone draining the Karakoram, Tethyan Himalaya and Kohistan–Ladakh Batholiths since the early Eocene (Clift, 2002). The Indus River's discharge is intensely seasonal due to the monsoon. The major

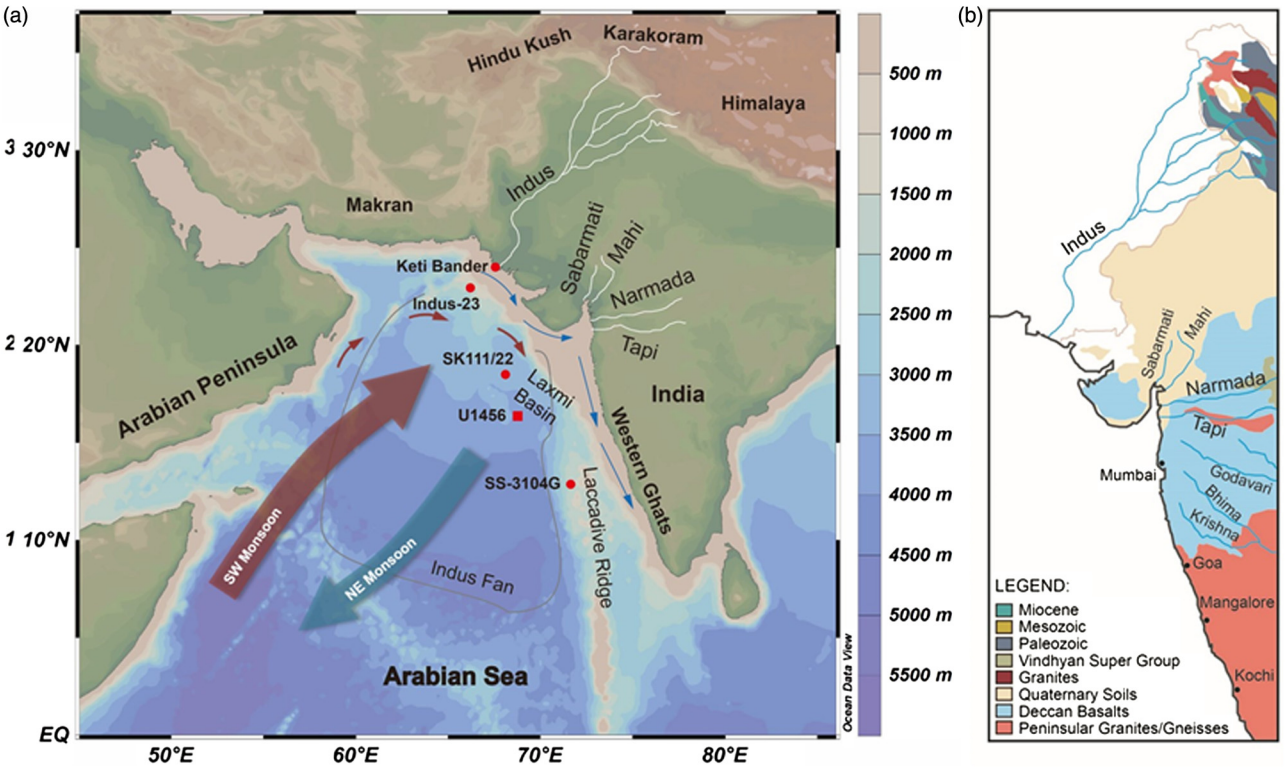


**Fig. 1.** (a) Bathymetric map of the Arabian Sea and the surrounding landmasses with monsoon climate. Red rectangle and circles represent IODP Site U1456 and sediment core sites of previous studies (Keti-Bandar, Indus-23, SK111/22, U1456, SS-3014G). Red and blue arrows show the surface and longshore currents. (b) Lithology of the drainage basins occupied by the different rivers in western India (modified after Kessarkar *et al.* 2003 and Goswami *et al.* 2012).

pulse occurs between April and October, caused by glacial melting and the summer monsoon precipitation (Karim & Veizer, 2002). The Indus River is also the largest source of sediment to the Arabian Sea; its annual sediment flux has been estimated at *c.* 250 million tons (Milliman & Syvitski, 1992). Most sediments from the Indus River are deposited and dispersed by the longshore current within the shallow continental shelf before being further transported onto the abyssal deep sea floor in the Arabian Sea (Clift *et al.* 2008; Limmer *et al.* 2012*a*). Both the Narmada and the Tapti Rivers also contribute more than ~125 million tons of sediments annually to the Arabian Sea (Milliman & Syvitski, 1992). Most of these sediments are distributed similarly along the inner continental shelves of western India (e.g. Avinash *et al.* 2016). The small rivers and streams in the Western Ghats discharge sediments into the Arabian Sea, but the sediment amounts are quite low, compared to the major rivers.

The provenance of detrital marine sediments encompasses both their formation by erosion of continental source rocks and the processes involved in their subsequent transportation and deposition on the sea floor. Sediment provenance studies have been conducted using diverse approaches such as geochemistry, sedimentology and mineralogy, providing information on many related topics: sediment sources, hydrographic and oceanographic processes, weathering intensity, and tectonic/crustal evolution at different timescales (e.g. McLennan & Taylor, 1991; Goldstein & Hemming, 2003; Grousset & Biscaye, 2005; Andrews & Eberl, 2012; Mazumder, 2017). The radiogenic Sr ($^{87}Sr/^{86}Sr$) and Nd ($^{143}Nd/^{144}Nd$) isotopes in detrital silicates are regarded as reliable fingerprints for sediment provenance, although there is some debate, such as whether chemical weathering may affect strontium isotopes, as to the importance of different factors in determining these ratios. The Sr and Nd isotopic composition of source rocks is decided by their Rb/Sr and Sm/Nd ratios, respectively, and by the ages of those source rocks. Thus, the Sr and Nd isotopic composition of detrital marine sediments which are the erosional products of continental rocks provides information on both the sediment source and the spatio-temporal variations in that source (e.g. Asahara *et al.* 1999; Colin *et al.* 1999, 2006; Innocent *et al.* 2000; Ahmad *et al.* 2005; Rutberg *et al.* 2005; Meyer *et al.* 2011; Tripathy *et al.* 2011; Goswami *et al.* 2012; Awasthi *et al.* 2014; Jonell *et al.* 2018).

Sediment provenance studies using several different approaches have been carried out in the Arabian Sea. Based on heavy mineral assemblages, Garzanti *et al.* (2005) reported that the sandy sediments in the northern and central Arabian Sea were supplied by the Indus River from the Himalaya, Transhimalaya and Karakoram ranges in northern India, whereas the sediment sources of deep sea sediments in the SE Arabian Sea were diverse. The main sources of the deep sea sediments were basic igneous rocks, gneisses/granites, high-grade metamorphic rocks, and sandstones in western and southwestern India (Akaram *et al.* 2015). In terms of clay minerals, Das *et al.* (2013) reported that the detrital fine-grained sediments in the SE Arabian Sea were supplied by numerous small rivers draining western India, and confirmed that the Holocene sediments along the western margin of India were divided regionally by distinct clay mineral associations representing the different sediment sources (Rao & Rao, 1995; Thamban *et al.* 2002; Kessarkar *et al.* 2003; Limmer *et al.* 2012*b*). Recently, Avinash *et al.* (2016) compiled multiple sediment proxies of the surface sediments in the eastern Arabian Sea, highlighting that the clay minerals in the shallow and deep sea sediments originate from different sources. Kessarkar *et al.* (2003)

https://doi.org/10.1017/S0016756818000596 Published online by Cambridge University Press

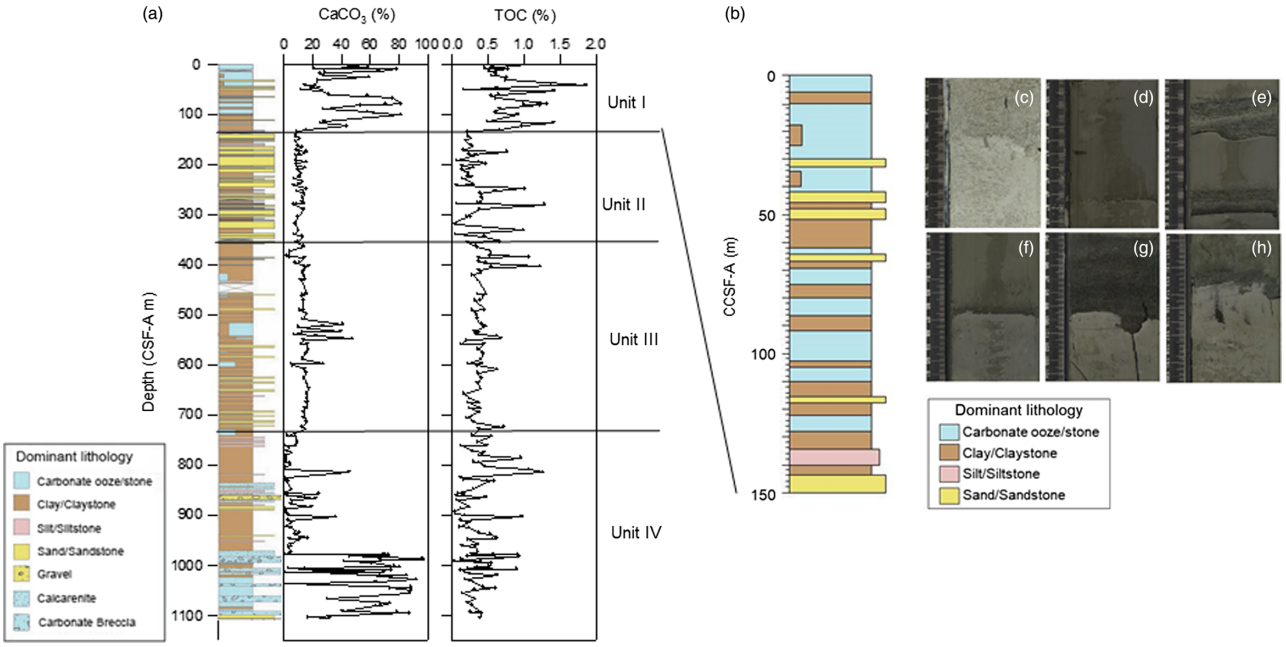


**Fig. 2.** (a) Lithostratigraphy of Site U1456 with down-core profiles of $CaCO_3$ and TOC contents. (b) Schematic columnar section of dominant lithologies of Unit I at Site U1456. (c) Calcareous ooze (Hole U1456A 12H-1, 22–32 cm). (d) Nannofossil-rich clay (Hole U1456A 4H-7, 38–48 cm). (e) Stacked turbidites showing normal grading (Hole U1456A 7H-5, 63–82 cm). (f) Sharp erosional boundary between thick layer of clay and interbedded thin silt layer (Hole U1456A 7H-4, 81–91 cm). (g) Erosional scoured surface at the top of nannofossil ooze (Hole U1456A 10H-4, 94–101 cm). (h) Nannofossil ooze turbidite containing oxidized pyrite (black spot) (Hole U1456A 10H-1, 110–120 cm). All figure panels are modified after Pandey *et al.* (2016).

first reported that Sr and Nd isotope data from many core sediments along the western margin of India constrained the possible sediment sources as well as changes in the degree of chemical weathering between the Holocene and the last glacial period. Later, Goswami *et al.* (2012) found a very narrow range of Sr and Nd isotopes, leading them to suggest that the provenance of these sediments remained unchanged during the last 40 ka in the eastern Arabian Sea. In addition, they proposed a possible supply of sediments from the Bay of Bengal to the SE Arabian Sea, in contrast to Kessarkar *et al.* (2003). Based on Sr and Nd isotopes in bulk sediments, Limmer *et al.* (2012*a*) confirmed that the Holocene sediments in the shallow continental shelf of NW India were mainly transported from the Indus River, despite being mixed with older sediments, emphasizing an active longshore transport in the NW part of the shelf (Shanas & Kumar, 2014). Different Sr and Nd isotopes of bulk sediments were reported from the major tributaries of the Indus River (Clift *et al.* 2002*a*, *b*) and the postglacial Indus delta (Clift *et al.* 2008).

Due to the large total amount of sediment discharge from the rivers, the Indus Fan is the main sediment repository in the Arabian Sea and contains a total of $\sim 5 \times 10^6$ km$^3$ in sediment volume, although it is only about one-third as large as its giant neighbour in the Bay of Bengal (Clift *et al.* 2001). Despite being smaller than the Bengal Fan, the Indus Fan covers $1.1 \times 10^6$ km$^2$, stretching 1500 km into the Indian Ocean, and the thickest point of the deposit is greater than 11 km (Clift *et al.* 2002*a*). Although the age of the Indus Fan remains a subject of debate, one theory is that the initiation of the fan formation was linked to the uplift of the Himalayas, and associated with sea-level lowering during the middle Oligocene to early Miocene (Clift *et al.* 2001). During the International Ocean Discovery Program (IODP) Expedition 355 in 2015, Site U1456 (16°37.28′ N, 68°50.33′ E, 3640 m of water depth) was drilled in Laxmi Basin in the eastern Arabian Sea (Fig. 1). Site U1456 is located offshore of the western margin of India, ~475 km from the Indian coast and ~820 km from the modern mouth of the Indus River. Drilling penetration at Site U1456 attained ~1109.4 m below sea floor (mbsf), reaching 13.5–17.7 Ma (late-early to early-middle Miocene), with only a few hiatuses (Pandey *et al.* 2016). Using the various kinds of sediment properties, lithologic units were defined on board based on a compilation of Holes U1456A to U1456E at Site U1456, in which each lithologic unit was characterized by a different depositional environment (Fig. 2a; Pandey *et al.* 2016). For example, Unit IV (>350 m thick), consisting of claystone and a mixture of light-grey calcarenite/calcilutite and grey breccia with conglomerate, is a massive mass transport deposit corresponding to the Nataraja submarine slide as identified from seismic reflection profiles along the Laxmi Basin (Calvès *et al.* 2015).

Although a variety of analytical tools have been used to elucidate the sediment provenance in the Arabian Sea, the reliability of various tools (e.g. clay minerals, elemental composition and detrital isotopes) in tracing sediment sources continues to be debated. In particular, although Clift & Blusztajn (2005) is an exception, most studies on sediment provenance have been limited to the last glacial period, and no information has been obtained on sediment provenance over the glacial–interglacial changes at orbital timescales. In this study, we measured Sr and Nd isotopes of the detrital fraction at IODP Site U1456 in the eastern Arabian Sea to trace changes in sediment provenance at the glacial–interglacial timescale over the last 800 ka.

## 2. Materials and methods

At IODP Site U1456, Lithologic Unit I, estimated as Pleistocene in age by the shipboard biostratigraphy (Pandey *et al.* 2016), forms a ~121 m thick sequence, consisting mainly of pelagic carbonates (nannofossil ooze and foraminifera-rich nannofossil ooze) interbedded with thin terrigenous layers (clay, silt and sand) showing planar lamination or massive structure (Fig. 2b). The sandy sediment layers are characterized by normal grading and sharp erosional bases and are interpreted as distal basin plain turbidites.

https://doi.org/10.1017/S0016756818000596 Published online by Cambridge University Press

The hemipelagic nannofossil ooze and nannofossil-rich clays are intensely bioturbated, and sometimes include common pyrite concretions (Fig. 2c–h). A total of 60 sediment samples were collected based on magnetic susceptibility (MS) changes at a discrete interval from a composite section (Holes U1456A and U1456C) of Unit I at Site U1456. All analytical data are summarized in Table 1 in the Supplementary Material (available at https://doi.org/10.1017/S0016756818000596).

The MS of sediments was measured non-destructively using a Bartington MS2C loop sensor equipped with the Whole-Round Multisensor Logger on board during the expedition (Pandey *et al.* 2016). Prior to grain-size analysis, detrital particles were isolated by removing organic matters and carbonates using diluted $H_2O_2$ and HCl, respectively. No step was taken to exclude biogenic opal because it was nearly absent from the samples. Grain-size analysis was conducted using standard sieves for the sand fractions and a Micromeritics SediGraph 5100D for the mud fractions. The mean grain size of detrital particles was calculated following the scheme of Folk & Ward (1957).

We measured the Sr and Nd isotopic compositions of the detrital fraction of the bulk sediments. These samples were prepared based on a sequential leaching method. In brief, dry bulk sediments were ground with an agate mortar, and ~1.0 g homogenized sediment samples were leached by 30 mL 1.5M buffered acetic acid for 4 hours at room temperature to remove carbonates. Fe–Mn oxides were then removed using 0.05M hydroxylamine hydrochloride – 25% acetic acid for 4 hours at a temperature of 85 °C (Bayon *et al.* 2002). Finally, biogenic silica was removed in 20 mL 1M sodium hydroxide solution for 30 min at a temperature of 80 °C. Each step includes centrifuging and triple rinses with ultrapure water, and the reagents used in the leaching were ultrapure grade. The final residues were dried in an oven at 50 °C, and ~50 mg of each dried sediment sample was dissolved in a 7 mL Teflon vial by digestion in a mixture of concentrated HF, $HNO_3$ and $HClO_4$ (TAMAPURE-AA-100 from Tama Chemicals, Ltd, Tokyo, Japan) for >18 hours on a hotplate (130–140 °C), in preparation for column chemistry.

Sr and Nd were refined by conventional column chemistry using cation-exchange resin (Mitsubishi diaion CK08P, 75–150 μm) with 1.8M HCl and Eichrom Ln-spec resin (50–100 μm) with 0.25M HCl for rare earth elements (Pin & Zalduegui, 1997). The total procedural blanks for Sr and Nd were negligible (0.05 ng and 0.25 ng, respectively) compared to the amount of Sr and Nd in the samples (>100 ng). Sr and Nd isotopic compositions were measured as $Sr^+$ on Ta single filament and $Nd^+$ on Re triple filaments with thermal ionization mass spectrometers (VG Sector 54-30 and GVI IsoProbe-T, respectively) at Nagoya University. During the measurement, a value of 0.710261 ± 0.000018 (2σ, $n$ = 12) was obtained for the international standard of $^{87}Sr/^{86}Sr$, NBS987. All Sr isotope ratios were corrected to an accepted value for the standard of 0.710250. During the measurement, for Nd isotopes, the average value obtained for the JNdi-1 standard was 0.512115 ± 0.000011 (IsoProbe-T, 2σ, $n$ = 16). The average of the standard runs of JNdi-1 was compared to the recommended value of JNdi-1 (0.512115) (Tanaka *et al.* 2000), and a correction factor was determined for each of the samples analysed on that day.

All reported $^{87}Sr/^{86}Sr$ and $^{143}Nd/^{144}Nd$ ratios were corrected for mass fractionation using $^{86}Sr/^{88}Sr$ = 0.1194 and $^{146}Nd/^{144}Nd$ = 0.7219, respectively. Nd isotope ratios are expressed as $\varepsilon_{Nd}$; $\varepsilon_{Nd}$ = parts per 10 000 variation of the $^{143}Nd/^{144}Nd$ ratio relative to the chondritic uniform reservoir ($^{143}Nd/^{144}Nd$ = 0.512638; Jacobsen & Wasserburg, 1980). Analytical errors ($^{87}Sr/^{86}Sr$: 0.00001, $\varepsilon_{Nd}$: 0.19) represent internal 2σ deviations of the mean (2SE).

## 3. Chronology

The preliminary age model for Site U1456 was determined on board based on biostratigraphy of calcareous nannofossil and planktonic foraminifera, together with magnetostratigraphy (Pandey *et al.* 2016). According to the succession of biostratigraphic events, the age of Site U1456 spans from the lower to middle Miocene to recent, with a few hiatuses (Fig. 2a). The age of Unit I was assigned to the Holocene to the middle Pleistocene. The overall sedimentation rate has been ~10 to ~12 cm $ka^{-1}$ since the late Pliocene, except for the early Pleistocene when the sedimentation rate reached ~45 cm $ka^{-1}$ during the deposition of Unit II.

A planktonic foraminiferal oxygen isotope stratigraphy was used to constrain the precise age model for Unit I (Fig. S1 in the Supplementary Material available at https://doi.org/10.1017/S0016756818000596). The details of the age model construction are described in Kim *et al.* (2018). Briefly, a total of 260 samples were collected from a composite section of Unit I consisting of Holes U1456A and U1456C. Oxygen isotope values of monospecific planktonic foraminifera (*Globigerinoides ruber*) were measured using Isoprime at the Center for Advanced Marine Core Research (Japan). Together with shipboard biostratigraphic and palaeomagnetic data at Site U1456, the established oxygen isotope stratigraphy of Unit I was correlated to LR04 stacks (Lisiecki & Raymo, 2005), in addition to the correlation of $\delta^{15}N$ values to ODP Hole 722B in the western Arabian Sea (Altabet, Murray & Prell, 1999). Consequently, the precise age constraint identifies that Unit I is younger than *c.* 1.2 Ma. The presence of frequent thin turbidite layers, particularly sandy turbidites, intercalated throughout the core makes the construction of a precise chronostratigraphy of Unit I more challenging (Fig. 2b). However, while uncertainty in the graphic correlation used to determine the glacial–interglacial boundaries may be of some importance, it does not significantly alter the interpretation of sediment provenance within the scheme of glacial–interglacial cycles used in this study. Finally, Figure S1 in the Supplementary Material (available at https://doi.org/10.1017/S0016756818000596) provides a continuous record extending down to ~1.2 Ma (Marine Isotope Stage (MIS) 36), with an average sedimentation rate of ~14 cm $ka^{-1}$, fluctuating between 5 and 32 cm $ka^{-1}$.

## 4. Results

The variations in Sr and Nd isotopic compositions in the detrital fraction of the bulk sediments from Unit I at Site U1456 are shown in Figure 3. The $^{87}Sr/^{86}Sr$ ratios and εNd values of Unit I vary from 0.711 to 0.726 and from −12.5 to −7.3, respectively. These results are comparable, although not identical, to the results of previous studies in the eastern Arabian Sea (Fig. 1; Kessarkar *et al.* 2003; Clift *et al.* 2008; Goswami *et al.* 2012; Limmer *et al.* 2012*a*). Sediments (<14 ka) from the Keti Bandar section drilled at the Indus River mouth are characterized by similar $^{87}Sr/^{86}Sr$ ratios (0.711–0.728) and slightly lower εNd values (−15.2 to −11.8) (Clift *et al.* 2010). Limmer *et al.* (2012*a*) reported that the εNd values (−12.3 to −10.1) of the Indus-23 core sediments (<1.5 ka) from the Indus Shelf are slightly higher than those of Keti Bandar, but they fall within the range of our results. The $^{87}Sr/^{86}Sr$ ratio and εNd value of a Holocene sediment from core SK111/22 (located north of Site U1456) are 0.717 and −14.6, whereas those of late Pleistocene sediment from that core are 0.716 and −17.3 (Kessarkar *et al.* 2003). Thus, the $^{87}Sr/^{86}Sr$ ratios of core SK111/22 are similar to our data, but εNd values are quite different. Goswami *et al.* (2012) reported that core SS-3104G which is located south of Site U1456 shows

https://doi.org/10.1017/S0016756818000596 Published online by Cambridge University Press

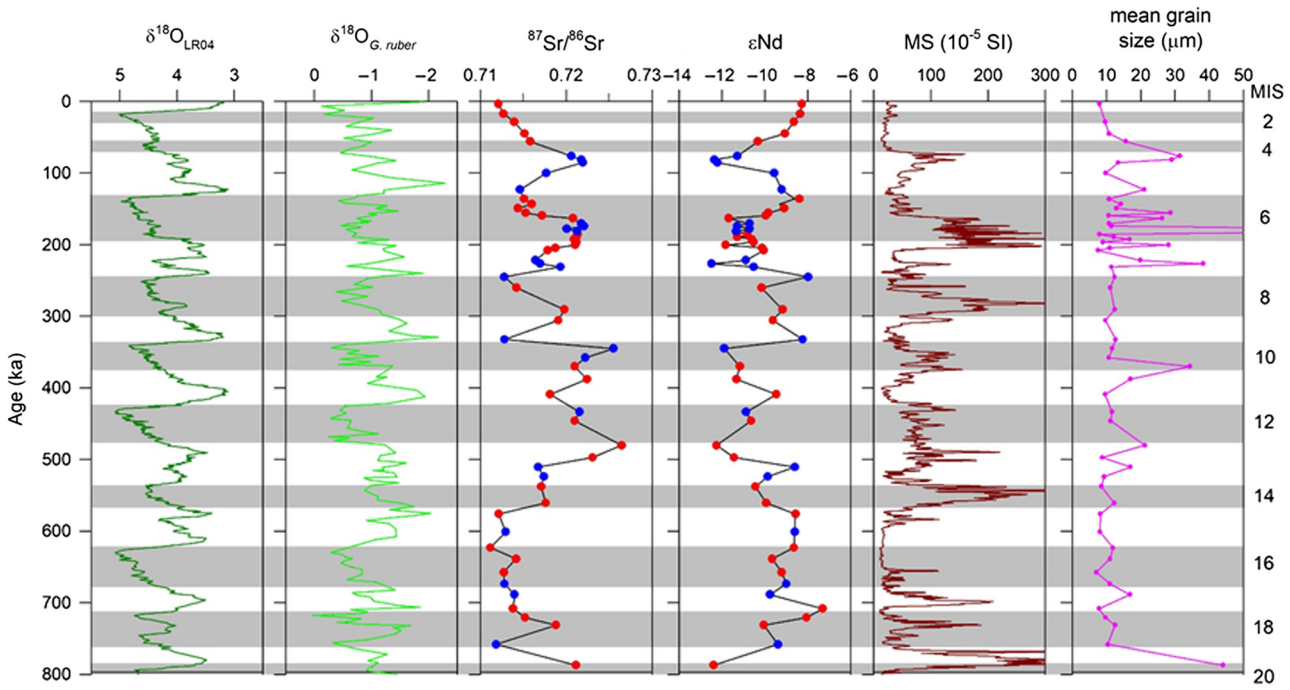


**Fig. 3.** Down-core profiles of $\delta^{18}$OLR04 (Lisiecki & Raymo, 2005), $\delta^{18}$O values of G. ruber (Kim *et al.* 2018), $^{87}Sr/^{86}Sr$ values, εNd ratios, magnetic susceptibility (MS), and mean grain size of Unit I at Site U1456 during the last 800 ka. The blue and red dots in the left panel are $\delta^{18}$O data from Holes U1456A and U1456C, respectively. The shading represents the glacial periods according to marine isotope stage (MIS).

$^{87}Sr/^{86}Sr$ ratios (0.714–0.718) and εNd values (−12.8 to −8.8) that are both quite similar to our results.

Variations in the pattern of $^{87}Sr/^{86}Sr$ ratios and εNd values of Unit I at Site U1456 appear to be quasi-cyclic during the last 800 ka (Fig. 3). However, these fluctuations are not clearly coincident with the glacial–interglacial cycles. Nonetheless, we observe systematic variations in the $^{87}Sr/^{86}Sr$ ratios and εNd values which display a nearly symmetrical variation pattern throughout the core. We also note that these variations are well correlated to MS variations (Fig. 4): low $^{87}Sr/^{86}Sr$ ratios and high εNd values coincide with low MS, whereas high $^{87}Sr/^{86}Sr$ ratios and low εNd values coincide with high MS. MS is related very closely to the concentration of terrestrial siliciclastic material; high MS correlates to low $CaCO_3$ layers whereas low MS correlates to high $CaCO_3$ layers (Fig. 2a; Pandey *et al.* 2016). The mean grain size in the detrital fraction mostly falls in the range 8–16 μm, except for several large grains up to 90 μm in size (Fig. 4). In some cases, the mean grain size is larger during high-MS intervals. The mean grain size is not closely related to the $^{87}Sr/^{86}Sr$ ratios, but does show a weak relationship with the low εNd values. The grain-size distribution pattern is classified into three types (Fig. S2 in the Supplementary Material available at https://doi.org/10.1017/S0016756818000596). The first type is the fine-grained sediments mostly between 10 and 100 μm. The second type is similar to the first type, but also includes a low content of coarse-grained sediments that are much coarser than the third type. The third type is characterized by the distinct peak of coarse-grained sediments comparable to the fine-grained sediments.

## 5. Discussion

### 5.a. Sediment provenance

#### 5.a.1. Sediment provenance of fluvial and marine sediments

The origins and source areas of the sediments in the eastern Arabian Sea offshore of the western coast of India have been documented in several previous studies (Rao & Rao, 1995; Thamban *et al.* 2002; Kessarkar *et al.* 2003; Garzanti *et al.* 2005; Goswami *et al.* 2012; Limmer *et al.* 2012*a*, *b*; Das *et al.* 2013; Akaram *et al.* 2015; Avinash *et al.* 2016; Jonell *et al.* 2018). Recently, studies using Sr and Nd isotopic composition of detrital silicates revealed the precise provenance of these sediments and the weathering history of the source silicates as a function of monsoon activity in the eastern Arabian Sea (e.g. Goswami *et al.* 2012). Similar studies had previously been carried out in neighbouring oceans such as the Bay of Bengal and the Andaman Sea (Colin *et al.* 1999, 2006; Ahmad *et al.* 2005; Tripathy *et al.* 2011; Awasthi *et al.* 2014; Joussain *et al.* 2016). It should be noted that tracing the sources of detrital marine sediments (and the spatio-temporal variations in those sources) using Sr and Nd isotopic composition requires assuming that the terrigenous marine sediments are the erosional products of continental basement rocks. Several lines of evidence support this assumption. Because early studies found an insignificant contribution to sediments from aeolian dust (e.g. Sirocko & Sarnthein, 1989), most sediments in the eastern Arabian Sea are thought to have been transported from the various rivers distributed along the western coast of India (e.g. Indus, Narmada, Tapi, Mahi and other small rivers and streams). For example, studies on clay minerals of surface sediments in the Arabian Sea documented that the dominant illite is principally derived from the Lesser Himalaya and Higher Himalaya (Kolla *et al.* 1976, 1981; Borole *et al.*, 1982), while the smectite is derived mostly from the Deccan Trap terrain (Ramaswamy *et al.* 1991) and subordinately from the Indus River (Alizai *et al.* 2012). However, the possibility of additional sediment transport by ocean current from the Bay of Bengal to the SE Arabian Sea is still under debate (Ramaswamy & Nair, 1989; Chauhan & Gujar, 1996; Kessarkar *et al.* 2003; Chauhan *et al.* 2010).

The Sr and Nd isotopic compositions of river sediments and drainage basin rocks in India have been reported by several previous studies (Peucat *et al.* 1989; Harris *et al.* 1994; Clift *et al.* 2002*a*, *b*,

https://doi.org/10.1017/S0016756818000596 Published online by Cambridge University Press

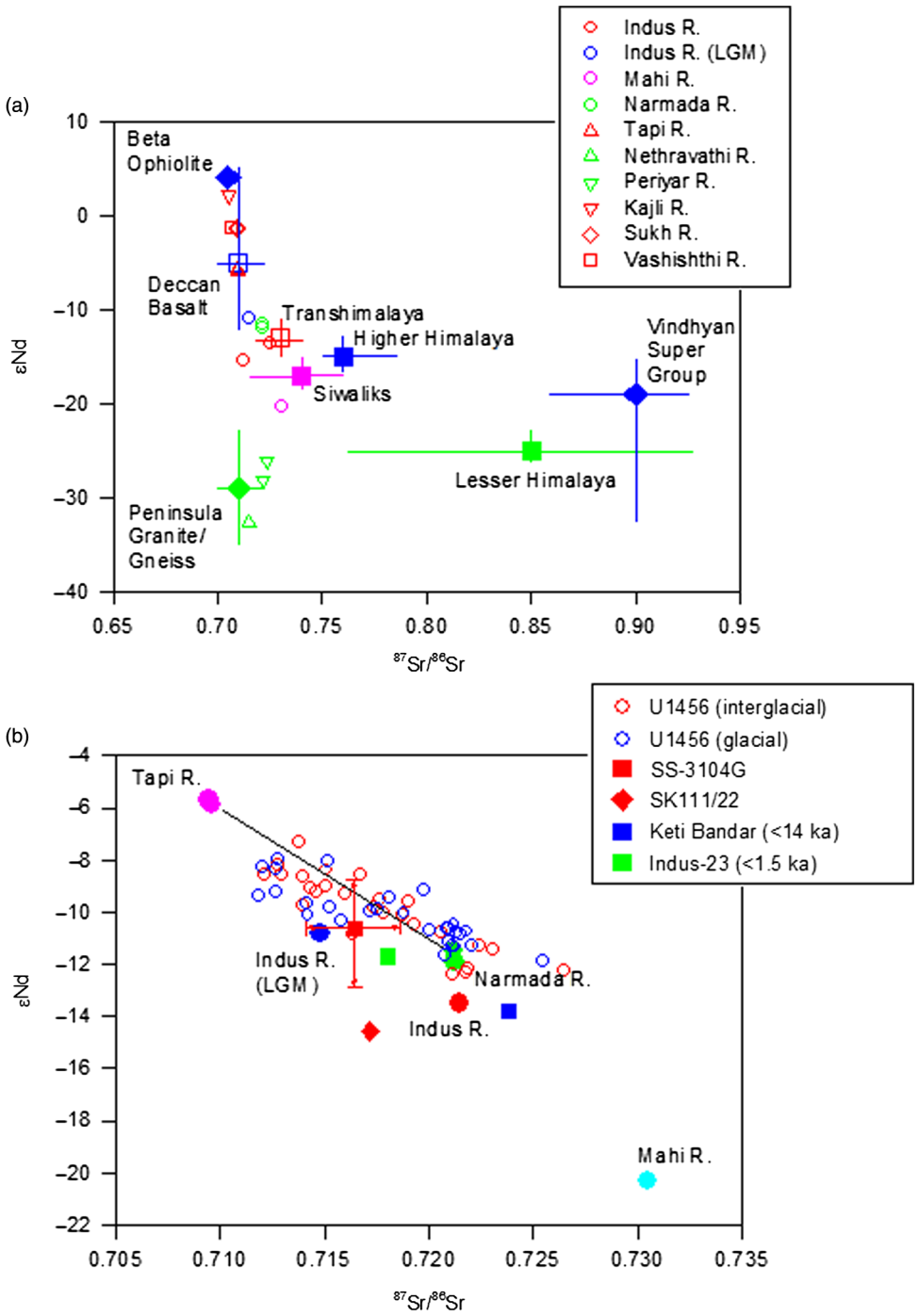


**Fig. 4.** (a) Biplot of $^{87}Sr/^{86}Sr$ values and εNd ratios of river sediments and drainage basin geologies of western India. Data were compiled from the literatures (Clift *et al.* 2008; Tripathy *et al.* 2011; Goswami *et al.* 2012; Limmer *et al.* 2012*a*). (b) Biplot of $^{87}Sr/^{86}Sr$ values and εNd ratios of Unit I at Site U1456 and published data from previous studies (Kessarkar *et al.* 2003; Clift *et al.* 2008, 2010; Goswami *et al.* 2012; Limmer *et al.* 2012*a*). Note that the red and blue circles in the lower panel represent the interglacial and glacial $^{87}Sr/^{86}Sr$ values and εNd ratios of samples at Site U1456.

2008, 2010; Chakrabarti *et al.* 2007; Singh *et al.* 2008; Ahmad *et al.* 2009; Tripathy *et al.* 2011; Goswami *et al.* 2012). These studies demonstrate that most river sediments have inherited the primary signature of Sr and Nd isotopic compositions from the drainage basin geology. Clift & Blusztajn (2005) reported that the evolution of the river drainage basin has altered the isotopic composition of river sediments. However, Chirouze *et al.* (2015) revealed that the earlier drainage capture model was incorrect. Figure 4a compiles all available Sr and Nd isotope data of river sediments and drainage basin rocks in India. For example, Clift *et al.* (2008) reported that the εNd values of the older rocks of the Indian craton and Lesser Himalaya are the most negative (−26 to −23), whereas those of the more primitive arc rocks of the Indus Suture Zone and Transhimalaya are somewhat positive (−1 to +8), and those of the Higher Himalaya and Karakoram are distinctly intermediate (−17 to −12 and −12 to −8, respectively). On the basis of the previous studies (Tripathy *et al.* 2011; Goswami *et al.* 2012; Limmer *et al.* 2012*a*) and the drainage basin geology of the rivers discharging into the eastern Arabian Sea, we selected several main end-member types represented by different lithologic components: Deccan Basalt ($^{87}Sr/^{86}Sr$; 0.71, εNd; −5.0); Peninsula Granite/Gneiss ($^{87}Sr/^{86}Sr$; 0.71, εNd; −29); Lesser Himalaya ($^{87}Sr/^{86}Sr$; 0.85, εNd; −25); Higher Himalaya ($^{87}Sr/^{86}Sr$; 0.76, εNd; −15); Vindhyan Super Group ($^{87}Sr/^{86}Sr$; 0.9, εNd; −19); and Bela Ophiolite ($^{87}Sr/^{86}Sr$; 0.71, εNd; +4.5).

The Indus River is very large (~2900 km long; basin area ~$10^6$ km$^2$). It flows from Tibet to the Arabian Sea, crossing

https://doi.org/10.1017/S0016756818000596 Published online by Cambridge University Press

the Western Himalayan Syntaxis, which was formed by the underthrusting of the Indian passive margin beneath the Asian active margin at ~55 Ma (Rowley, 1996; Najman *et al.* 2010; DeCelles *et al.* 2014). The Indus River is composed of numerous large tributaries draining a largely elevated and tectonically active basin occupying western Tibet, the Tethyan Himalaya (Lesser Himalaya and Higher Himalaya) and the Karakoram, known as the Indus Suture Zone (Fig. 1a; Inam *et al.* 2007). Clift *et al.* (2002*b*) reported that the εNd values of sediments collected in the different areas of the Indus River drainage basin reliably correspond to the signature of the basement being drained, although εNd values of the Indus River system are extremely diverse, varying from −30 to −1. The modern Indus River sediments are thought to be supplied mainly from the exhumation of the Lesser Himalaya (41%) and/or Higher Himalaya (38%) with Karakoram/Transhimalaya (19%), although the relative contributions have changed substantially since the Last Glacial Maximum (Clift *et al.* 2008). Other major rivers such as the Narmada and the Tapi drain different geological areas (Fig. 1b). The Narmada flows through the Vindhyan Super Group and the Deccan Basalt (Gupta *et al.* 2011), whereas the Tapi River largely passes through the Deccan Basalt (Kale *et al.* 2003). The $^{87}Sr/^{86}Sr$ ratios and εNd values of the small rivers and streams discharged from the Western Ghats are also set by their drainage basin characteristics (Goswami *et al.* 2012).

The possible different sediment sources to Site U1456 in the Laxmi Basin have characteristic Sr and Nd isotopic compositions (Fig. 4b). The Tapi River supplies sediments of less radiogenic Sr (0.710) and more radiogenic Nd (−5.8) isotopes, representing a sediment source influenced by the Deccan Basalt. The Mahi River discharges sediments characterized by the most radiogenic Sr (0.731) and quite unradiogenic Nd (−20.3) isotopes because it drains multi-lithological terrain consisting of the Vindhyan Super Group, the Deccan Basalt and other metamorphic rocks (Sridhar, 2008). The $^{87}Sr/^{86}Sr$ ratio and εNd values of the Indus River (0.722 and −13.5) and Narmada River (0.721 and −11.9) are somewhat similar, although these two rivers pass through totally different lithologic drainage basins (Fig. 1b). The Indus River sediments are eroded mostly from the Higher Himalaya and/or Lesser Himalaya, but the Narmada River sediments contain contributions from both the Vindhyan Super Group, with more radiogenic Sr and unradiogenic Nd isotopes, and the Deccan Basalt, with less radiogenic Sr and highly radiogenic Nd isotopes. Clift *et al.* (2008) suggested from the Indus Delta drilling at Keti Bandar (Fig. 1a) that the εNd value of the Indus River was more radiogenic (−10.8) during the last glacial period. The decrease of the εNd value toward −14.0 during the Holocene was attributed, not to drainage reorganization, but to an increase in erosion in the Lesser Himalaya due to intensified summer monsoon precipitation and a decrease in the erosion of terrains in the Indus Suture Zone (which were dominant during the last glacial period) (Clift *et al.* 2010). Both the glacial sediments of the Indus Delta and the surface sediments in the deep sea Indus Canyon showed a similar εNd value (−10.8), demonstrating that the Indus River discharge during the last glacial period had a different isotopic composition from the interglacial value (Clift *et al.* 2008).

Our results confirm the previous studies (Garzanti *et al.* 2005; Avinash *et al.* 2016), suggesting that the Unit I sediments at Site U1456 have multiple provenances (Fig. 4b). Interestingly, $^{87}Sr/^{86}Sr$ ratios and εNd values of sediments are not divided distinctly following the glacial and interglacial cycles, suggesting that the sediment provenance did not change systematically between the glacial and interglacial periods at Site U1456. The linear correlation between the Sr and Nd isotope compositions of these sediments reflects the dominant contributions of two important end-members: one is the Narmada and Indus Rivers and the other is the Tapi River. Although the Mahi River discharges sediments with the most radiogenic Sr and fairly unradiogenic Nd isotopes in the north of the Narmada River, its contribution to Site U1456 seems to be minor. It is difficult to distinguish between the Narmada and Indus Rivers on the basis of $^{87}Sr/^{86}Sr$ ratios and εNd values, and thus the relative contributions of the individual rivers cannot be estimated. Use of another tracer might allow for differentiation between the two rivers. The contribution of sediment discharge by the Narmada River seems to be more significant than that of the Indus River. As mentioned above, the $^{87}Sr/^{86}Sr$ ratio and εNd value of the glacial sediments of the Indus River (Clift *et al.* 2008) differ somewhat from the Holocene sediments (Fig. 4b). Although precipitation and river discharge decreased during the glacial period due to the enhanced winter monsoon, the role of the Indus River during the glacial period when the sea level was low should not be dismissed. Therefore, the $^{87}Sr/^{86}Sr$ ratio and εNd value clearly indicate that the sediments in the Laxmi Basin of the eastern Arabian Sea have been supplied from the Tapi River, Narmada River and Indus River during the last 800 ka. In addition, variation of these isotope values is not related to orbital-scale glacial and interglacial cycles that closely influenced the monsoon strength and its sediment discharge. We note that Avinash *et al.* (2016) also reported that the deep sea surficial sediments of the eastern Arabian Sea are influenced by different terrigenous sources, including the Indus–Narmada–Tapti Rivers and southern Indian rivers, based on the spatial distribution patterns of various sediment provenance proxies (environmental magnetism, geochemistry, particle size and clay mineralogy).

Our results are comparable to other published $^{87}Sr/^{86}Sr$ ratios and εNd values of sediments in the eastern Arabian Sea (Fig. 4b), although direct comparison of these data may be biased due to differences in analytical procedures, the absence or presence of carbonate, and the selection of bulk sediments versus fine fractions. The previously reported $^{87}Sr/^{86}Sr$ ratios and εNd values of the modern Indus Delta at Keti Bandar (<14 ka) are a little higher and lower, respectively, than those reported here, because these isotopes only represent inputs from the Indus River (Clift *et al.* 2010). Kessarkar *et al.* (2003) also reported that the Holocene sediments of core SK111/22 were mainly transported from the Indus River, but their $^{87}Sr/^{86}Sr$ ratios and εNd values were higher and slightly lower, respectively, than those of Keti Bandar (<14 ka) and Site U1456 (Fig. 4b). The main reason for this discrepancy may be the measurement of different sediment grain sizes, because Kessarkar *et al.* (2003) used the fine-grained (<2 μm) fraction. Another possible reason is more sediment flux from the Deccan Plateau to the core site SK111/22. Although core Indus-23 (<1.5 ka) was recovered from the Indus Shelf offshore of the Indus River mouth, its $^{87}Sr/^{86}Sr$ ratios and εNd values are less and more radiogenic, respectively, than those of Keti Bandar at the modern Indus Delta (Limmer *et al.* 2012*a*). The lower $^{87}Sr/^{86}Sr$ ratios of Indus-23 (<1.5 ka) from the Indus Shelf may result from the higher carbonate content in that core leading to a supplementary isotopic contribution to the detrital fraction. In contrast, slightly higher εNd values of Indus-23 (<1.5 ka) reflect an additional contribution from a different sediment source (i.e. Bela Ophiolite; Fig. 5a). The data also indicate that the Sr and Nd isotope compositions of the shallow Indus Shelf (Limmer *et al.* 2012*a*) display a much wider range than those of the Indus River, and the isotopic compositions of the deep sea Indus Canyon are close to those of the Indus River (Li *et al.* 2015). The $^{87}Sr/^{86}Sr$ ratios and εNd values of core SS-3104G, which covers the past 40 ka, overlap

https://doi.org/10.1017/S0016756818000596 Published online by Cambridge University Press

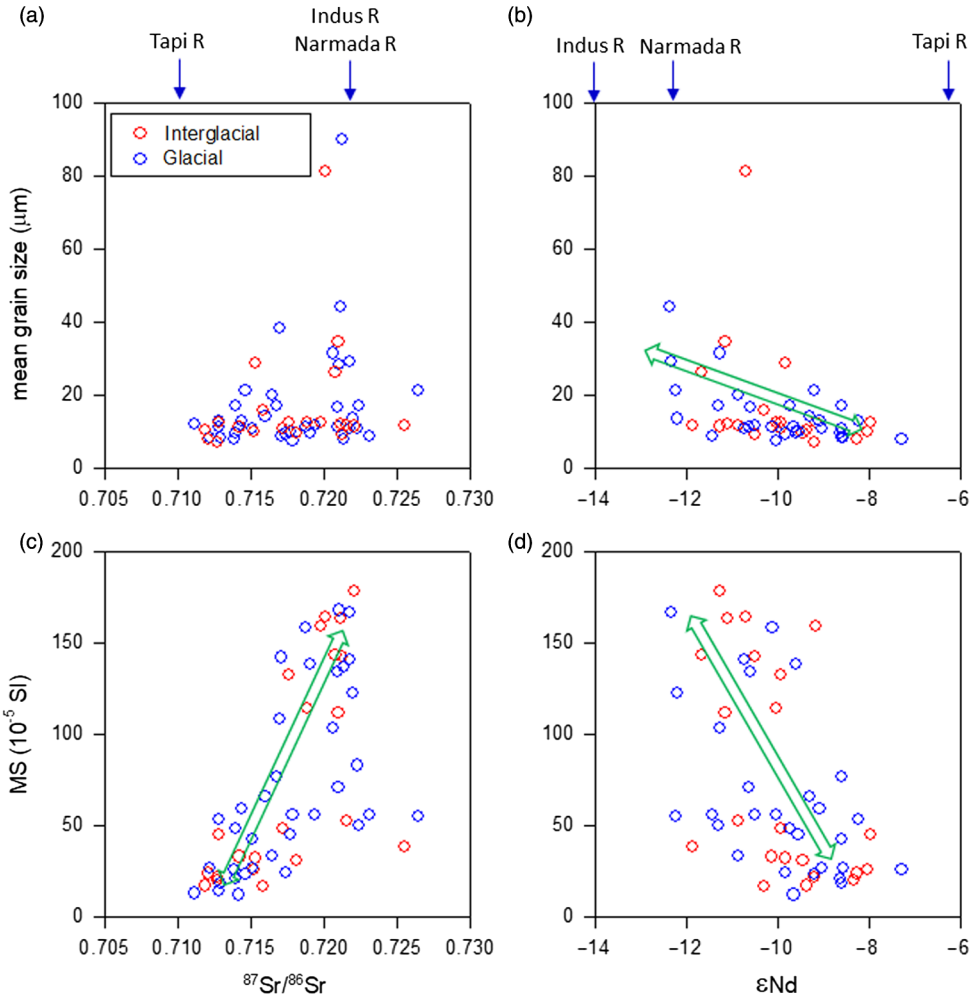


**Fig. 5.** (a) Correlation between mean grain size and $^{87}Sr/^{86}Sr$ values of Unit I. (b) Correlation between mean grain size and εNd ratios of Unit I. (c) Correlation between magnetic susceptibility (MS) and $^{87}Sr/^{86}Sr$ values of Unit I. (d) Correlation between MS and εNd ratios of Unit I. Note that the red and blue circles the interglacial and glacial samples. The locations in this space of the sediment provenance signatures of the rivers considered here are marked by blue arrows above the figure.

closely with our results (Fig. 4b). According to Goswami *et al.* (2012), the very narrow range of isotope variation in core SS-3104G in the eastern Arabian Sea suggests that many rivers should be considered as potential sources (such as the Indus, Narmada and Tapi including other Western Ghats streams).

Since the collision between the Indian Plate and Eurasia, the modern Indus River's drainage basin systems have mostly developed within the tectonic blocks of the Indus Suture Zone. Roddaz *et al.* (2011) measured the Sr–Nd isotopic composition of middle Eocene to early Miocene rocks in the Himalaya region, revealing a shift toward more radiogenic Sr–Nd isotopic compositions as the result of the exhumation and erosion of the Tethyan Himalaya. Older (50–30 Ma) sedimentary deposits were subject to larger contributions from the Karakoram and the Tethyan Himalaya, whereas the major contributions to the younger (30–15 Ma) sedimentary deposits were from the Tethyan belt and the Higher Himalayan Crystallines, with smaller contributions from the Karakoram, Ophiolitic Suture (mostly Kohistan) and Transhimalaya (Roddaz *et al.* 2011). Thus, the evolution of the Indus River drainage basin indicates that the Sr–Nd isotope signatures of the sediments allow discrimination between the older (50–30 Ma; 0.708–0.712, −9.8 to −8.5) and younger (30–15 Ma; 0.712–0.724, −13.3 to −9.9) periods. Clift *et al.* (2001) reported εNd values of Indus Fan sediments at DSDP Site 224 in the Owen Ridge of the western Arabian Sea. The authors found that the εNd values at DSDP Site 224 are very similar between the middle Eocene to middle Oligocene (from −13.1 to −10.9 and mean *c.* −11.9) and the late Oligocene to early Miocene (from −12.4 to −11.1 and mean *c.* −11.5). This implies that from the middle Eocene to early Miocene, the Indus River sediments were eroded mainly within the drainage north of the Indus Suture Zone. Based on the εNd values of industrial well Indus Marine A-1, however, Clift & Blusztajn (2005) discovered that a dramatic switch in Nd isotopic character occurred after 5 Ma, decreasing toward −15 (i.e. the εNd value of the modern Indus Delta sand; Clift *et al.* 2002*b*), although this value (−15) is a little lower than that of the modern river in the mixing calculation plot (Fig. 4b). This change in the εNd value is attributed to a rerouting of the major tributaries of the Indus River within the drainage basin, supplying more erosional products from the Himalayan sources. However, this model of widespread drainage rearrangement is contradicted by the recent finding that the isotopic shift was caused by enhanced erosion of rocks in the Nanga Parbat syntaxis (Chirouze *et al.* 2015). Nonetheless, our results validate the assumption that over the study interval of the last 800 ka, the Indus River has not undergone a route shift in the drainage, and thus the sediment provenance has remained consistent.

### 5.a.2. Effects on detrital sediment isotopes

As summarized by Blum & Erel (2003), it is well established that the Sr isotopic ratios of detrital particles are more dependent on the grain size than Nd isotopes, especially in the case of aeolian dust. The main control on the relationship between Sr and Nd isotopic compositions and grain size may be geochemical processes, as Rb

https://doi.org/10.1017/S0016756818000596 Published online by Cambridge University Press

and Sr have different reaction rates, but the reaction rates between Sm and Nd are similar. Since it was first reported by Dasch (1969), the increase of $^{87}Sr/^{86}Sr$ ratios with decreasing grain size of aeolian dust has been confirmed repeatedly due to the fractionation during the chemical weathering (Asahara *et al.* 1999; Cole *et al.* 2009; Feng *et al.* 2009). Recently, Jonell *et al.* (2018) reported that $^{87}Sr/^{86}Sr$ ratios of fine-grained size fraction in the Indus Delta sediments are attributed to K-feldspar, mica, epidote and/or volcanic clay minerals. In our study $^{87}Sr/^{86}Sr$ ratios and mean grain size are entirely unrelated (Fig. 5a). Thus, sediment provenance is a more important factor for controlling $^{87}Sr/^{86}Sr$ ratios than the hydrodynamic sorting or grain-size fraction at Site U1456. In this study, analytical error of replicates shows that $\Delta^{87}Sr/^{86}Sr$ is only 0.00001. Because we did not measure $^{87}Sr/^{86}Sr$ ratios for the grain-size fraction, the uncertainties in Sr isotopic measurement cannot be estimated. If we adopt uncertainties of $\Delta^{87}Sr/^{86}Sr$ values (0.01243) from Jonell *et al.* (2018), the variation (0.15) of $\Delta^{87}Sr/^{86}Sr$ values at Site U1456 exceeds the uncertainties, emphasizing that the sediment provenance change played a critical role in $\Delta^{87}Sr/^{86}Sr$ values.

Most studies have shown that Nd isotopic ratios were known to be unaffected by particle size (e.g. Meyer *et al.* 2011), but the influence of grain size on Nd isotope ratios was demonstrated by Jonell *et al.* (2018), showing that different mineralogy of grain-size fraction controls Nd isotopic compositions. For example, high εNd values of the fine-grained size fraction are due to monazite and allanite, whereas low εNd values of coarse-grained size fraction are controlled by mica. In this study, εNd values show a relationship with mean grain size in which the coarse-grained particles are characterized by less radiogenic Nd isotopes (Fig. 5b). This trend contradicts the results of Jonell *et al.* (2018) in the Indus Delta. The opposite trend between this study and Jonell *et al.* (2018) may be the different component of sediment provenances. Jonell *et al.* (2018) examined the bulk sediments of mono sediment provenance in the Indus Delta, whereas this study reveals that the sediment provenances are mixed in the Laxmi Basin.

Comparing εNd values among the Indus Canyon, Indus Shelf, Indus River mouth, and suspended clay-rich sediment from the modern Indus River (Goldstein *et al.* 1984; Clift *et al.* 2002*b*, 2008, 2010), Limmer *et al.* (2012*a*) also raised the possibility of grain-size control on Nd isotope character, but deemed it unlikely as they did not find a correlation between εNd values and Si/Al ratios. However, the εNd values measured from the <2 μm size fraction of core SK111/22 are lower than those measured from bulk sediments in other cores such as Site 1456 and the previously studied cores (SS-3104G, Keti Bandar, and Indus-23) (Fig. 4b). Without chemical composition data for bulk sediments, we cannot test the validity of grain-size control on Nd isotope composition. Regardless, grain-size control on Nd isotopic composition is unlikely to be straightforward, as shown by the opposite revealed by this study and Jonell *et al.* (2018). While most previous studies on sediment provenance using Sr–Nd isotopes have used bulk sediments or a specific size fraction, the incorporation of individual detritus grains into bulk sediments may depend on the grain size (e.g. Holz *et al.* 2007). Furthermore, we note that sediment transport processes are grain-size dependent, such that different grain-size fractions in discharged river-derived materials may be preferentially transported to different depositional sites. The analytical error of replicates in this study is *c.* 0.19 for $\Delta\varepsilon_{Nd}$. As in the case of the $^{87}Sr/^{86}Sr$ ratios, the uncertainties in εNd values related to grain size cannot be estimated. However, the uncertainties of $\Delta\varepsilon_{Nd}$ values (0.6) reported by Jonell *et al.* (2018) are insignificant, compared to the variation (5.2) of $\Delta\varepsilon_{Nd}$ values at Site U1456. Thus, our results confirm that the sediments in the Laxmi Basin are mixed by different sediment provenances.

Although the long-term evolution of monsoon strength is mainly controlled by tectonic uplift (Clift *et al.* 2010), short-term changes in monsoon strength are caused primarily by the glacial–interglacial cycles. The Arabian Sea experiences the strong SW monsoon during summer, with very high rainfall (>3000 mm). The degree of chemical weathering may increase during warmer and wetter conditions such as summer monsoon (Valdiya, 1999; West *et al.* 2005). $^{87}Sr/^{86}Sr$ ratios of detrital silicates have been used to track the degree of chemical weathering, because Sr is released more easily than Rb from the source rocks during chemical weathering (e.g. Blum & Erel, 2003). In contrast, Nd isotopes are unaffected by chemical weathering, and thus εNd values of detrital particles have been regarded as reliable indicators for the provenance of terrigenous particles (e.g. Blum & Erel, 2003). For example, in the Andaman Sea and the Bay of Bengal, Colin *et al.* (1999) reported that the interglacial sediments are characterized by similar εNd values and lower $^{87}Sr/^{86}Sr$ ratios than the glacial sediments, which is attributed to more chemical weathering during sediment transportation under the warm and wet climate conditions during the interglacial period. Limmer *et al.* (2012*b*) investigated the degree of chemical weathering in the Indus Shelf of the northern Arabian Sea and reported that the period of the maximum summer monsoon corresponds to stronger chemical weathering, based on the multi-proxy mineral record showing high smectite/(illite+chlorite) ratio, low illite crystallinity and high hematite/goethite ratio. More intense chemical weathering was confirmed by the negative correlation between $^{87}Sr/^{86}Sr$ and K/Al ratios (Limmer *et al.* 2012*a*). However, it should be noted that their samples include the carbonate fraction and that these data were limited to ages younger than 15 ka. Thus, it is difficult to conclude with certainty that the degree of chemical weathering follows the glacial–interglacial cycles. Monsoon rains also play an important role in controlling erosional pattern in the river drainage basin at least over orbital and even millennial timescales. Because the Indus River drainage is affected by the summer monsoon precipitation (Bookhagen & Burbank, 2006), Clift *et al.* (2010) suggested that the rain shadow moves between the Lesser Himalaya and the Higher Himalaya following the glacial–interglacial cycles. However, the $^{87}Sr/^{86}Sr$ ratios and εNd values at Site U1456 do not show a clear glacial–interglacial cyclic pattern, which implies that another factor may influence these variations (Fig. 4). For example, the influence of sea level differed between the shallow water delta of earlier studies and the deep basin of this study, by buffering the sediments in the delta during high sea level and reworking during low sea level.

### 5.b. Implications for the relationship between sediment provenance and depositional processes

At Site U1456, Unit I consists mainly of pelagic carbonates (nannofossil ooze and foraminifera-rich nannofossil ooze) interbedded with thin terrigenous (clay, silt and sand) layers (Fig. 2b), representing the pelagic sedimentation and distal turbidite deposition in the Indus Fan, respectively (Pandey *et al.* 2016). The carbonate-rich pelagic sediments and clastic-rich turbidite layers are distinguished by MS, which is generally higher for the terrigenous sediments than for the carbonate sediments (Fig. 3). The relationships are clearly shown in Figure 5c and d: the high-MS intervals (i.e. turbidites) correspond to high $^{87}Sr/^{86}Sr$ ratios and low εNd values, whereas the low-MS intervals (i.e. pelagic sediments) coincide with low $^{87}Sr/^{86}Sr$ ratios and high εNd values (Fig. 3). Figure 5c, d also shows that the high-MS sediments (i.e. turbidite deposition)

https://doi.org/10.1017/S0016756818000596 Published online by Cambridge University Press

characterized by high $^{87}Sr/^{86}Sr$ ratios and low εNd values are associated with the sediment provenances of the Indus River and an unknown additional input from the Narmada River, whereas the low-MS sediments (i.e. pelagic sedimentation) characterized by low $^{87}Sr/^{86}Sr$ ratios and high εNd values are likely related to the sediment provenance of the Tapi River. Thus, the $^{87}Sr/^{86}Sr$ ratios and εNd values of the detrital fraction at Unit I of Site U1456 may be controlled not only by the sediment provenance but also by depositional processes (pelagic sedimentation versus turbidite deposition) mainly controlled by orbital-scale sea-level change.

In the submarine fan system, sediments are transported from the shallow continental shelf to the deep sea floor via deep sea channels or submarine canyons (e.g. McHargue & Webb, 1986). It is through these channels and canyons that the turbidity current flows to transport the sediments. The turbidity current, rather than the basinward transfer of suspended material bypassing the continental shelves, is the main depositional process involved in building the deep sea fan (e.g. Bourget *et al.* 2013). Kolla & Coumes (1987) reported numerous high-relief channel/levee systems rather on the continental slope and rise. Furthermore, based on a high-resolution multi-beam swath bathymetry survey in the middle of the Indus Fan, Mishra *et al.* (2015) revealed the presence of sinuous channel systems that play an important role in transporting sediments toward the distal submarine fan. Analogously to the Bengal Fan, the turbidity currents are the dominant depositional processes in the formation of the Indus Fan, although the submarine scar and mass slump deposits were observed and the pelagic sedimentation occurs during the cessation of turbidite sedimentation in the Indus Fan (e.g. Rodriguez *et al.* 2011, 2012). Thus, it is clear that growth of the Indus Fan depends on sediment transport by the turbidity current as well as on the by-passing of pelagic suspension to the deep sea floor. Increasing sediment transport by turbidity currents may have played a more important role under low-sea-level conditions, when the river channel and canyon advanced toward the deeper part of the basin. In contrast, during high-sea-level conditions, most of the sediments were trapped in the shallow marine environment, preventing the turbidity current from transporting the sediments to the deep sea basin, and instead allowing pelagic sedimentation to become the dominant contributor to the growth of the Indus Fan. For example, Clift & Giosan (2014) reported the sediment budget during the Holocene sea-level stand, such as approximately half of the sediments in the shallow marine environment and the other half under the terrestrial delta, with <1% entering the submarine canyon.

The evolution of large river-fed turbidite systems in the Indus Fan is closely related to the glacio-eustatic sea-level change and position of the deltaic shoreline (von Rad & Tahir, 1997; Mouchot *et al.* 2010; Bourget *et al.* 2013). For example, Bourget *et al.* (2013) established turbidite stratigraphy in the Owen Fracture Zone (20° N pull-apart basin) of the western Arabian Sea and emphasized the importance of sea-level control on sediment transfer through the channel–levee systems in forming these Indus River-fed megaturbidites. In addition, Prins *et al.* (2000) reported that the upper fan of the Indus Fan ceased activity after 10 ka. At the short-term (i.e. orbital) timescale, the development of the turbidite system in the Indus Fan may have been generally activated by enhanced sediment loads resulting from increased run-off from a mixture of monsoon precipitation and snow melt, because glacial and fluvially reworked detritus was easily eroded from the high-relief, rapidly uplifting mountains (Giosan *et al.* 2006). At Site U1456, turbidite layers occurred frequently during the glacial periods, but some turbidites were also found during the interglacial periods (Fig. 3). Thus, the linkage between the development of turbidites and climate-induced sediment transfer in the Indus sedimentary system is not always consistent. Similarly, Bourget *et al.* (2013) reported that the relationship between 20° N Basin megaturbidites and the Indian Summer Monsoon stack of Caley *et al.* (2011) was poorly organized. Nevertheless, it is clear that the turbidite deposits characterized by high $^{87}Sr/^{86}Sr$ ratios and low εNd values reflect more sediment transport from the Indus and/or Narmada Rivers (Fig. 5c and d).

Prins *et al.* (2000) reported that thin pelagic sediments were interbedded within thick turbidite depositions at ODP Site 720 in the Owen Ridge of the western Arabian Sea. In contrast, at Unit I of Site U1456 in the eastern Arabian Sea, thin turbidite layers were interbedded within thick pelagic sediments (Fig. 2b). These pelagic sediments contain high $CaCO_3$ contents consisting mainly of biogenic particles (Pandey *et al.* 2016), clearly reflecting a decrease in clastic influx during sea-level highstand. The reduced terrigenous sediments may be a result of channel switching, abandonment or burial of active channel. Kolla & Coumes (1987) discovered a major eastward shift of active channel deposition in the Indus Fan during the Pleistocene sea-level lowering. In addition, the different types of grain-size distribution patterns represent the degree of mixing between the detrital fine-grained and coarse-grained particles (Fig. S2 in the Supplementary Material available at https://doi.org/10.1017/S0016756818000596) as suggested by Dietze *et al.* (2012). Furthermore, Clift *et al.* (2008) reported that since *c.* 11 ka, different εNd values have characterized the surface sediments of deep sea Indus Canyon and the Indus River, suggesting that the Indus River could not supply sediments to the canyon and submarine fan under high-sea-level conditions (Prins & Postma, 2000). At Site U1456 in the Laxmi Basin, the pelagic sedimentation is more closely related to the increase of palaeoproductivity than to the decrease of terrigenous particles. In general, palaeoproductivity in the Arabian Sea increased during the interglacial periods when the SW monsoon was intensified (Thamban *et al.* 2001; Pattan *et al.* 2003; Banakar *et al.* 2005; Avinash *et al.* 2015; Naik *et al.* 2017). During pelagic sedimentation, detrital particles characterized by low $^{87}Sr/^{86}Sr$ ratios and high εNd values might be more strongly influenced by the Tapi River (Fig. 5), although we leave determination of the precise reason for the isotopic separation between the turbidites and pelagic sediments to future studies. The crucial factor for the isotopic separation seems to be the amount of discharge from peninsular India, compared to the Indus River.

## 6. Conclusions

The Arabian Sea is well known for its seasonal monsoon climate and, relatedly, the huge sedimentary deposit known as the Indus Fan. IODP Expedition 355 drilled to 1109.4 m penetration at Site U1456 in the Laxmi Basin of the eastern Arabian Sea. The uppermost Unit I (~121 m thick) of the drilled sedimentary sequence consists mainly of pelagic carbonates (nannofossil ooze and foraminifera-rich nannofossil ooze) interbedded with thin terrigenous (clay, silt and sand) layers. Together with the shipboard biostratigraphic and palaeomagnetic data of Site U1456, age determination by the correlation of $\delta^{18}O$ fluctuations of planktonic foraminifera (*G. ruber*) to LR04 stacks shows that Unit I spans ~1.2 Ma covering MIS 36. $^{87}Sr/^{86}Sr$ ratios and εNd values of detrital particles vary from 0.711 to 0.726 and from −12.5 to −7.3, respectively, during the last 800 ka. Although the variation patterns of $^{87}Sr/^{86}Sr$ ratios and εNd values appear quasi-cyclic, these fluctuations do not coincide with the glacial–interglacial cycles. The

https://doi.org/10.1017/S0016756818000596 Published online by Cambridge University Press

fairly linear correlation between εNd and $^{87}Sr/^{86}Sr$ clearly indicates the contributions of two major end-members (the Indus and Narmada versus the Tapi) to these sediments. By considering the εNd and $^{87}Sr/^{86}Sr$ end-members of possible river sediment sources, we found that the Tapi River is responsible for sediments with low $^{87}Sr/^{86}Sr$ ratios and high εNd values whereas the Narmada and Indus Rivers are the main contributors to sediments with high $^{87}Sr/^{86}Sr$ ratios and low εNd values. Glacial sediments from the Indus River may play a secondary role, while the Mahi River is not likely to supply a significant fraction. The mean grain size of the detrital fraction falls for the most part between 8 and 16 μm, except for several large grains reaching up to 90 μm in size. In some cases, high-MS intervals are associated with large mean grain sizes. The mean grain size is not closely related to $^{87}Sr/^{86}Sr$ ratios, confirming that the grain size is not a major control on the $^{87}Sr/^{86}Sr$ ratios. However, the εNd values display a relationship with mean grain size. As supporting data are lacking, the possibility of grain-size control on Nd isotope character cannot be further explored at this time. Finally, low $^{87}Sr/^{86}Sr$ ratios and high εNd values are correlated to low MS, whereas high $^{87}Sr/^{86}Sr$ ratios and low εNd values are correlated to high MS. Because MS depends on the relative amount of the detrital fraction, high MS correlates to turbidite deposits whereas low MS is closely related to high $CaCO_3$ pelagic sediments. The $^{87}Sr/^{86}Sr$ ratios and εNd values of the detrital fraction in the Laxmi Basin of the Arabian Sea may reflect not only the sediment provenance, but also the depositional processes at play (turbidite deposition versus pelagic sedimentation) including the amount of fine-grained sediments from peninsular India and the Deccan Traps.

**Supplementary material.** To view supplementary material for this article, please visit https://doi.org/10.1017/S0016756818000596.

**Acknowledgements.** This research used samples provided by IODP, and data collected on board the vessel *JOIDES Resolution* (IODP Expedition 355-Arabian Sea Monsoon). The editor-in-chief (Dr Peter Clift), Dr Jean-Carloss Montero-Serrano and an anonymous reviewer are all appreciated for their constructive comments to improve the data interpretation. This research was supported by the National Research Foundation of Korea grants (2016K2A9A2A08003704, 2016R1A2B4008256) and K-IODP of the Korean government.

## References

**Ahmad S, Anil Babu G, Padmakumari V, Dayal A, Sukhija B and Nagabhushanam P** (2005) Sr, Nd isotopic evidence of terrigenous flux variations in the Bay of Bengal: implications of monsoons during the last ~34,000 years. *Geophysical Research Letters* **32**, L2271. doi: 10.1029/2005GL024519.

**Ahmad SM, Padmakumari V and Babu GA** (2009) Strontium and neodymium isotopic compositions in sediments from Godavari, Krishna and Pennar rivers. *Current Science* **97**, 1766–9.

**Akaram V, Das S, Rai A and Mishra G** (2015) Heavy mineral variation in the deep sea sediment of southeastern Arabian Sea during the past 32 kyr. *Journal of Earth System Science* **124**, 477–86.

**Alagarsamy R and Zhang J** (2005) Comparative studies on trace metal geochemistry in Indian and Chinese rivers. *Current Science* **89**, 299–309.

**Alizai A, Hillier S, Clift PD and Giosan L** (2012) Clay mineral variations in Holocene terrestrial sediments from the Indus Basin; a response to SW Asian Monsoon variability. *Quaternary Research* **77**, 368–81.

**Altabet MA, Murray DW and Prell WL** (1999) Climatically linked oscillations in Arabian Sea denitrification over the past 1 my: implications for the marine N cycle. *Paleoceanography* **14**, 732–43.

**Andrews JT and Eberl, DD** (2012) Determination of sediment provenance by unmixing the mineralogy of source-area sediments: the "SedUnMix" program. *Marine Geology* **291**, 24–33.

**Asahara Y, Tanaka T, Kamioka H, Nishimura A and Yamazaki T** (1999) Provenance of the north Pacific sediments and process of source material transport as derived from Rb–Sr isotopic systematics. *Chemical Geology* **158**, 271–91.

**Avinash K, Kurian, PJ, Warrier AK, Shankar R, Vineesh T and Ravindra R** (2016) Sedimentary sources and processes in the eastern Arabian Sea: insights from environmental magnetism, geochemistry and clay mineralogy. *Geoscience Frontiers* **7**, 253–64.

**Avinash K, Manjunath BR and Kurian PJ** (2015) Glacial-interglacial productivity contrasts along the eastern Arabian Sea: dominance of convective mixing over upwelling. *Geoscience Frontiers* **6**, 913–25.

**Awasthi N, Ray JS, Singh AK, Band ST and Rai VK** (2014) Provenance of the Late Quaternary sediments in the Andaman Sea: implications for monsoon variability and ocean circulation. *Geochemistry, Geophysics, Geosystems* **15**, 3890–906.

**Banakar VK, Oba T, Chodankar AR, Kuramoto T, Yamamoto M and Minagawa M** (2005) Monsoon related changes in sea surface productivity and water column denitrification in the Eastern Arabian Sea during the last glacial cycle. *Marine Geology* **219**, 99–108.

**Bayon G, German C, Boella R, Milton J, Taylor R and Nesbitt R** (2002) An improved method for extracting marine sediment fractions and its application to Sr and Nd isotopic analysis. *Chemical Geology* **187**, 179–99.

**Blum J and Erel Y** (2003) Radiogenic isotopes in weathering and hydrology. In *Surface and Ground Water, Weathering, and Soils* (ed. JI Drever), pp. 365–9. Treatise on Geochemistry, vol. 5. Oxford: Elsevier-Pergamon.

**Borole D, Sarin M and Somayajulu B** (1982) Composition of Narbada and Tapti estuarine particles and adjacent Arabian Sea sediments. *Indian Journal of Marine Science* **11**, 51–62.

**Bookhagen B and Burbank DW** (2006) Topography, relief, and TRMM-derived rainfall variations along the Himalaya. *Geophysical Research Letters* **33**, L08405. doi: 10.1029/2006GL026037.

**Bourget J, Zaragosi S, Rodriguez M, Fournier M, Garlan T and Chamot-Rooke N** (2013) Late Quaternary megaturbidites of the Indus Fan: origin and stratigraphic significance. *Marine Geology* **336**, 10–23.

**Caley T, Malaizë B., Zaragosi S, Rossignol L, Bourget J, Eynaud F, Martinez P, Giraudeau J, Charlier K and Ellouz-Zimmermann N** (2011) New Arabian Sea records help decipher orbital timing of Indo-Asian monsoon. *Earth and Planetary Science Letters* **308**, 433–44.

**Calvès G, Huuse M, Clift PD and Brusset S** (2015) Giant fossil mass wasting off the coast of West India: the Nataraja submarine slide. *Earth and Planetary Science Letters* **432**, 265–72.

**Chakrabarti R, Basu AR and Chakrabarti A** (2007) Trace element and Nd-isotopic evidence for sediment sources in the mid-Proterozoic Vindhyan Basin, central India. *Precambrian Research* **159**, 260–74.

**Chandramohan T and Balchand A** (2007) Regional sediment yield pattern for the west flowing rivers of Kerala State, India. *Materials and Geoenvironment* **54**, 501–11

**Chauhan OS and Gujar A** (1996) Surficial clay mineral distribution on the southwestern continental margin of India: evidence of input from the Bay of Bengal. *Continental Shelf Research* **16**, 321–33.

**Chauhan OS, Dayal A, Basavaiah N and Kader U** (2010) Indian summer monsoon and winter hydrographic variations over past millennia resolved by clay sedimentation. *Geochemistry, Geophysics, Geosystems* **11**, Q09009. doi: 10.1029/2010GC003067.

**Chirouze F, Huyghe P, Chauvel C, van der Beek P, Bernet M and Mugnier JL** (2015) Stable drainage pattern and variable exhumation in the Western Himalaya since the Middle Miocene. *Journal of Geology* **123**, 1–20.

**Clift PD** (2002) A brief history of the Indus River. In *The Tectonic and Climatic Evolution of the Arabian Sea Region* (eds PD Clift, D Kroon, C Gaedicke and J Craig), pp. 237–58. Geological Society of London, Special Publication no. 195.

**Clift PD and Blusztajn J** (2005) Reorganization of the western Himalayan river system after five million years ago. *Nature* **438**, 1001–3.

**Clift P, Gaedicke C, Edwards R, Lee JI, Hildebrand P, Amjad S, White RS and Schlüter H-U** (2002*a*) The stratigraphic evolution of the Indus Fan and the history of sedimentation in the Arabian Sea. *Marine Geophysical Researches* **23**, 223–45.

**Clift PD and Giosan L** (2014) Sediment fluxes and buffering in the post-glacial Indus Basin. *Basin Research* **26**, 369–86.

**Clift PD, Giosan L, Blusztajn J, Campbell IH, Allen C, Pringle M, Tabrez AR, Danish M, Rabbani M and Alizai A** (2008) Holocene erosion of the Lesser Himalaya triggered by intensified summer monsoon. *Geology* **36**, 79–82.

**Clift PD, Giosan L, Carter A, Garzanti E, Galy V, Tabrez AR, Pringle M, Campbell IH, France-Lanord C and Blusztajn J** (2010) Monsoon control over erosion patterns in the western Himalaya: possible feed-back into the tectonic evolution. In *Monsoon Evolution and Tectonic-Climate Linkage in Asia* (eds PD Clift, R Tada and H Zheng), pp. 185–218. Geological Society of London, Special Publication no. 342.

**Clift PD, Lee JI, Hildebrand P, Shimizu N, Layne GD, Blusztajn J, Blum JD, Garzanti E and Khan AA** (2002*b*) Nd and Pb isotope variability in the Indus River System: implications for sediment provenance and crustal heterogeneity in the Western Himalaya. *Earth and Planetary Science Letters* **200**, 91–106.

**Clift PD, Shimizu N, Layne G, Blusztajn J, Gaedicke C, Schlüter H-U, Clark M and Amjad S** (2001) Development of the Indus Fan and its significance for the erosional history of the Western Himalaya and Karakoram. *Geological Society of America Bulletin* **113**, 1039–51.

**Cole JM, Goldstein SL, Hemming SR and Grousset FE** (2009) Contrasting compositions of Saharan dust in the eastern Atlantic Ocean during the last deglaciation and African Humid Period. *Earth and Planetary Science Letters* **278**, 257–66.

**Colin C, Turpin L, Bertaux J, Desprairies A and Kissel C** (1999) Erosional history of the Himalayan and Burman ranges during the last two glacial–interglacial cycles. *Earth and Planetary Science Letters* **171**, 647–60.

**Colin C, Turpin L, Blamart D, Frank N, Kissel C and Duchamp S** (2006) Evolution of weathering patterns in the Indo-Burman Ranges over the last 280 kyr: effects of sediment provenance on 87Sr/86Sr ratios tracer. *Geochemistry, Geophysics, Geosystems* 7, Q03007. doi: 10.1029/2005GC000962.

**Das SS, Rai AK, Akaram V, Verma D, Pandey A, Dutta K and Prasad GR** (2013) Paleoenvironmental significance of clay mineral assemblages in the southeastern Arabian Sea during last 30 kyr. *Journal of Earth System Science* **122**, 173–85.

**Dasch EJ** (1969) Strontium isotopes in weathering profiles, deep-sea sediments, and sedimentary rocks. *Geochimica et Cosmochimica Acta* **33**, 1521–52.

**Decelles PG, Kapp P, Gehrels GE and Ding L** (2014) Paleocene-Eocene foreland basin evolution in the Himalaya of southern Tibet and Nepal: implications for the age of initial India-Asia collision. *Tectonics* **33**, 824–49.

**Dietze E, Hartmann K, Diekmann B, Ijmker J, Lehmkuhl F, Opitz S, Stauch G, Wünnemann B and Borchers A** (2012) An end-member algorithm for deciphering modern detrital processes from lake sediments of Lake Donggi Cona NE Tibetan Plateau, China. *Sedimentary Geology* **243/244**, 169–80.

**Feng J-L, Zhu L-P, Zhen X-L and Hu Z-G** (2009) Grain size effect on Sr and Nd isotopic compositions in eolian dust: implications for tracing dust provenance and Nd model age. *Geochemical Journal* **43**, 123–31.

**Folk RL and Ward WC** (1957) Brazos River bar: a study in the significance of grain size parameters. *Journal of Sedimentary Research* **27**, 3–26.

**Garzanti E, Vezzoli G, Ando S, Paparella P and Clift PD** (2005) Petrology of Indus River sands: a key to interpret erosion history of the Western Himalayan Syntaxis. *Earth and Planetary Science Letters* **229**, 287–302.

**Giosan L, Constantinescu S, Clift PD, Tabrez AR, Danish M and Inam A** (2006) Recent morphodynamics of the Indus delta shore and shelf. *Continental Shelf Research* **26**, 1668–84.

**Goldstein SL and Hemming SR** (2003) Long-lived isotopic tracers in oceanography, paleoceanography, and ice-sheet dynamics. In *The Oceans and Marine Geochemistry* (eds HD Holland and KK Turekian), pp. 453–89. Treatise on Geochemistry, vol. 6. Oxford: Elsevier-Pergamon.

**Goldstein S, O'nions R and Hamilton P** (1984) A Sm–Nd isotopic study of atmospheric dusts and particulates from major river systems. *Earth and Planetary Science Letters* **70**, 221–36.

**Goswami V, Singh SK, Bhushan R and Rai VK** (2012) Temporal variations in $^{87}Sr/^{86}Sr$ and εNd in sediments of the southeastern Arabian Sea: impact of monsoon and surface water circulation. *Geochemistry, Geophysics, Geosystems* **13**, Q01001. doi: 10.1029/2011GC003802.

**Grousset FE and Biscaye PE** (2005) Tracing dust sources and transport patterns using Sr, Nd and Pb isotopes. *Chemical Geology* **222**, 149–67.

**Gupta H, Chakrapani GJ, Selvaraj K and Kao S-J** (2011) The fluvial geochemistry, contributions of silicate, carbonate and saline–alkaline components to chemical weathering flux and controlling parameters: Narmada River (Deccan Traps), India. *Geochimica et Cosmochimica Acta* **75**, 800–24.

**Haake B, Ittekkot V, Rixen T, Ramaswamy V, Nair R and Curry W** (1993) Seasonality and interannual variability of particle fluxes to the deep Arabian Sea. *Deep-Sea Research I* **40**, 1323–44.

**Harris N, Santosh M and Taylor P** (1994) Crustal evolution in South India: constraints from Nd isotopes. *The Journal of Geology* **102**, 139–50.

**Holz C, Stuut J-BW, Henrich R and Meggers H** (2007) Variability in terrigenous sedimentation processes off northwest Africa and its relation to climate changes: inferences from grain-size distributions of a Holocene marine sediment record. *Sedimentary Geology* **202**, 499–508.

**Inam A, Clift PD, Giosan L, Tabrez AR, Tahir M, Rabbani MM and Danish M** (2007) The geographic, geological and oceanographic setting of the Indus River. In *Large Rivers: Geomorphology and Management* (ed. A Gupta), pp. 333–46. New York: John Wiley & Sons, Ltd.

**Innocent C, Fagel N and Hillaire-Marcel C** (2000) Sm–Nd isotope systematics in deep-sea sediments: clay-size versus coarser fractions. *Marine Geology* **168**, 79–87.

**Jacobsen SB and Wasserburg GJ** (1980) Sm–Nd isotopic evolution of chondrites. *Earth and Planetary Science Letters* **50**, 139–55.

**Jonell TN, Li Y, Blusztajn J, Giosan L and Clift PD** (2018) Signal or noise? Isolating grain size effects on Nd and Sr isotope variability in Indus delta sediment provenance. *Chemical Geology* **485**, 56–73.

**Joussain R, Colin C, Liu Z, Meynadier L, Fournier L, Fauquembergue K, Zaragosi S, Schmidt F, Rojas V and Bassinot F** (2016) Climatic control of sediment transport from the Himalayas to the proximal NE Bengal Fan during the last glacial-interglacial cycle. *Quaternary Science Reviews* **148**, 1–16.

**Kale VS, Mishra S and Baker VR** (2003) Sedimentary records of palaeofloods in the bedrock gorges of the Tapi and Narmada rivers, central India. *Current Science* **84**, 1072–9.

**Karim A and Veizer J** (2002) Water balance of the Indus River Basin and moisture source in the Karakoram and western Himalayas: implications from hydrogen and oxygen isotopes in river water. *Journal of Geophysical Research: Atmospheres* **107**, 4362. doi: 10.1029/2000JD000253.

**Kessarkar PM, Rao VP, Ahmad S and Babu GA** (2003) Clay minerals and Sr–Nd isotopes of the sediments along the western margin of India and their implication for sediment provenance. *Marine Geology* **202**, 55–69.

**Kim JE, Khim BK, Ikehara M and Lee J** (2018) Orbital-scale denitrification changes in the Eastern Arabian Sea during the last 800 kyrs. *Scientific Reports* **8**, 7072.

**Kolla V and Coumes F** (1987) Morphology, internal structure, seismic stratigraphy, and sedimentation of Indus Fan. *American Association of Petroleum Geologists Bulletin* **71**, 650–77.

**Kolla V, Henderson L and Biscaye PE** (1976) Clay mineralogy and sedimentation in the western Indian Ocean. *Deep-Sea Research* **23**, 949–61.

**Kolla V, Kostecki J, Robinson F, Biscaye P and Ray P** (1981) Distributions and origins of clay minerals and quartz in surface sediments of the Arabian Sea. *Journal of Sedimentary Research* **51**, 563–9.

**Li Y, Clift PD, Boening P, Guilderson T and Giosan L** (2015) Controls on sediment flux through the Indus Submarine Canyon during the Last Glacial Cycle. In Society of Exploration Geophysicists Annual Meeting, 18–23 October 2015, New Orleans, Louisiana USA (ed. RV Schneider), pp. 1907–11.

**Limmer DR, Böning P, Giosan L, Ponton C, Köhler CM, Cooper MJ, Tabrez AR and Clift PD** (2012*a*) Geochemical record of Holocene to Recent sedimentation on the Western Indus continental shelf, Arabian Sea. *Geochemistry, Geophysics, Geosystems* **13**, Q01008. doi: 10.1029/2011GC003845.

**Limmer DR, Köhler CM, Hillier S, Moreton SG, Tabrez AR and Clift PD** (2012*b*) Chemical weathering and provenance evolution of Holocene–recent sediments from the Western Indus Shelf, Northern Arabian Sea inferred from physical and mineralogical properties. *Marine Geology* **326**, 101–15.

**Lisiecki LE and Raymo ME** (2005) A Pliocene-Pleistocene stack of 57 globally distributed benthic $\delta^{18}O$ records. *Paleoceanography* **20**, PA1003. doi: 10.1029/2004PA001071.

**Mazumder R** (2017) *Sediment Provenance: Influences on Compositional Change from Source to Sink*. Amsterdam: Elsevier, 600 pp.

**McHargue TR and Webb JE** (1986) Internal geometry, seismic facies, and petroleum potential of canyons and inner fan channels of the Indus submarine fan. *American Association of Petroleum Geologists Bulletin* **70**, 161–80.

**McLennan S and Taylor S** (1991) Sedimentary rocks and crustal evolution: tectonic setting and secular trends. *The Journal of Geology* **99**, 1–21.

**Meyer I, Davies GR and Stuut JBW** (2011) Grain size control on Sr-Nd isotope provenance studies and impact on paleoclimate reconstructions: an example from deep-sea sediments offshore NW Africa. *Geochemistry, Geophysics, Geosystems* **12**, Q03005. doi: 10.1029/2010GC003355.

**Milliman J, Quraishee G and Beg M** (1984) Sediment discharge from the Indus River to the ocean: past, present and future. In *Marine Geology and Oceanography of Arabian Sea and Coastal Pakistan* (eds BU Haq and JD Milliman), pp. 65–70. New York: Van Nostrand Reinhold.

**Milliman JD and Syvitski JP** (1992) Geomorphic/tectonic control of sediment discharge to the ocean: the importance of small mountainous rivers. *The Journal of Geology* **100**, 525–44.

**Mishra R, Pandey DK, Ramesh P and Shipboard Scientific Party SK-306** (2015) Active channel system in the middle Indus fan: results from high-resolution bathymetry surveys. *Current Science* **108**, 409–12.

**Mooley DA and Parthasarathy B** (1984) Fluctuations in all-India summer monsoon rainfall during 1871–1978. *Climatic Change* **6**, 287–301.

**Mouchot N, Loncke L, Mahieux G, Bourget J, Lallemant S, Ellouz-Zimmermann N and Leturmy P** (2010) Recent sedimentary processes along the Makran trench (Makran active margin, off Pakistan). *Marine Geology* **271**, 17–31.

**Naik DK, Saraswat R, Lea DW, Kurtarkar SR and Mackensen A** (2017) Last glacial-interglacial productivity and associate changes in the eastern Arabian Sea. *Palaeogeography, Palaeoclimatology, Palaeoecology* **483**, 147–56.

**Nair R, Ittekkot V, Manganini S, Ramaswamy V, Haake B, Degens E, Desai BT and Honjo S** (1989) Increased particle flux to the deep ocean related to monsoons. *Nature* **338**, 749–51.

**Najman Y, Appel E, Boudagher-Fadel M, Bown P, Carter A, Garzanti E, Godin L, Han J, Liebke U, Oliver G, Parrish R and Vezzoli G** (2010) Timing of India-Asia collision: geological, biostratigraphic, and palaeomagnetic constraints. *Journal of Geophysical Research (Solid Earth)* **115**, B12416. doi: 10.1029/2010JB007673.

**Pandey DK, Clift PD, Kulhanek DK and the Expedition 355 Scientists** (2016) Site U1456. *The Proceedings of the International Ocean Discovery Program* **355**, 1–61.

**Pattan JN, Masuzawa T, Naidu PD, Parthiban G and Yamamoto M** (2003) Productivity fluctuations in the southeastern Arabian Sea during the last 140 ka. *Palaeogeography, Palaeoclimatology, Palaeoecology* **193**, 575–90.

**Peucat J, Vidal P, Bernard-Griffiths J and Condie K** (1989) Sr, Nd, and Pb isotopic systematics in the Archean low-to high-grade transition zone of southern India: syn-accretion vs. post-accretion granulites. *The Journal of Geology* **97**, 537–49.

**Pin C and Zalduegui JS** (1997) Sequential separation of light rare-earth elements, thorium and uranium by miniaturized extraction chromatography: application to isotopic analyses of silicate rocks. *Analytica Chimica Acta* **339**, 79–89.

**Prins MA and Postma G** (2000) Effects of climate, sea level, and tectonics unraveled for last deglaciation turbidite records of the Arabian Sea. *Geology* **28**, 375–8.

**Prins MA, Postma G, Cleveringa J, Cramp A and Kenyon N** (2000) Controls on terrigenous sediment supply to the Arabian Sea during the late Quaternary: the Indus Fan. *Marine Geology* **169**, 327–49.

**Ramaswamy V and Nair R** (1989) Lack of cross-shelf transport of sediments on the western margin of India: evidence from clay mineralogy. *Journal of Coastal Research* **5**, 541–6.

**Ramaswamy V, Nair R, Manganini S, Haake B and Ittekkot V** (1991) Lithogenic fluxes to the deep Arabian Sea measured by sediment traps. *Deep-Sea Research* **38**, 169–84.

**Rao VP and Rao BR** (1995) Provenance and distribution of clay minerals in the sediments of the western continental shelf and slope of India. *Continental Shelf Research* **15**, 1757–71.

**Roddaz M, Said A, Guillot S, Antoine P-O, Montel J-M, Martin F and Darrozes J** (2011) Provenance of Cenozoic sedimentary rocks from the Sulaiman fold and thrust belt, Pakistan: implications for the palaeogeography of the Indus drainage system. *Journal of the Geological Society* **168**, 499–516.

**Rodriguez M, Fournier M, Chamot-Rooke N, Huchon P, Bourget J, Sorbier M, Zaragosi S and Rabaute A** (2011) Neotectonics of the Owen Fracture Zone (NW Indian Ocean): structural evolution of an oceanic strike-slip plate boundary. *Geochemistry, Geophysics, Geosystems* **12**, Q12006. doi: 10.1029/2011GC003731.

**Rodriguez M, Fournier M, Chamot-Rooke N, Huchon P, Zaragosi S and Rabaute A** (2012) Mass wasting processes along the Owen Ridge (Northwestern Indian Ocean). *Marine Geology* **326/328**, 80–100.

**Rowley DB** (1996) Age of initiation of collision between India and Asia: a review of stratigraphic data. *Earth and Planetary Science Letters* **145**, 1–13.

**Rutberg RL, Goldstein SL, Hemming SR and Anderson RF** (2005) Sr isotope evidence for sources of terrigenous sediment in the southeast Atlantic Ocean: is there increased available Fe for enhanced glacial productivity? *Paleoceanography* **20**, PA1018. doi: 10.1029/2003PA000999.

**Shanas PR and Kumar V** (2014) Coastal processes and longshore sediment transport along Kundapura coast, central west coast of India. *Geomorphology* **214**, 436–51.

**Shankar R, Subbarao K and Kolla V** (1987) Geochemistry of surface sediments from the Arabian Sea. *Marine Geology* **76**, 253–79.

**Singh SK, Rai SK and Krishnaswami S** (2008) Sr and Nd isotopes in river sediments from the Ganga Basin: sediment provenance and spatial variability in physical erosion. *Journal of Geophysical Research: Earth Surface* **113**, F03006. doi: 10.1029/2007JF000909.

**Sirocko F and Sarnthein M** (1989) Wind-borne deposits in the northwestern Indian Ocean: record of Holocene sediments versus modern satellite data. In *Paleoclimatology and Paleometeorology: Modern and Past Patterns of Global Atmospheric Transport* (eds M Leinen and M Sarnthein), pp. 401–33. NATO ASI Series (Series C: Mathematical and Physical Sciences), vol. **282**.

**Sridhar A** (2008) Evidence of a late-medieval mega flood event in the upper reaches of the Mahi River basin, Gujarat. *Current Science* **96**, 1517–20.

**Tanaka T, Togashi S, Kamioka H, Amakawa H, Kagami H, Hamamoto T, Yuhara M, Orihashi Y, Yoneda S and Shimizu H** (2000) JNdi-1: a neodymium isotopic reference in consistency with LaJolla neodymium. *Chemical Geology* **168**, 279–81.

**Thamban M, Rao VP and Schneider R** (2002) Reconstruction of late Quaternary monsoon oscillations based on clay mineral proxies using sediment cores from the western margin of India. *Marine Geology* **186**, 527–39.

**Thamban M, Rao VP, Schneider RR and Grootes PM** (2001) Glacial to Holocene fluctuations in hydrography and productivity along the southwestern continental margin of India. *Palaeogeography, Palaeoclimatology, Palaeoecology* **165**, 113–27.

**Tripathy GR, Singh SK, Bhushan R and Ramaswamy V** (2011) Sr–Nd isotope composition of the Bay of Bengal sediments: impact of climate on erosion in the Himalaya. *Geochemical Journal* **45**, 175–86.

**Valdiya KS** (1999) Rising Himalaya: advent and intensification of monsoon. *Current Science* **76**, 514–24.

**von Rad U and Tahir M** (1997) Late Quaternary sedimentation on the outer Indus shelf and slope (Pakistan): evidence from high-resolution seismic data and coring. *Marine Geology* **138**, 193–236.

**West AJ, Galy A and Bickle M** (2005) Tectonic and climatic controls on silicate weathering. *Earth and Planetary Science Letters* **235**, 211–28.

https://doi.org/10.1017/S0016756818000596 Published online by Cambridge University Press